nature communications

Article

https://doi.org/10.1038/s41467-025-65897-4

Enhancing CAR- and TCR-mediated targeting of cancer via an immune synapse-stabilizing receptor

Received: 1 July 2024

Accepted: 27 October 2025

Published online: 04 February 2026

Check for updates

Chiou-Tsun Tsai[1,2], Jorge Ibanez-Vega[3], Pan Yin[1], Robert Teis[3,4], Norihiro Watanabe[1], Tadahiro Honda[1], Mikhail Valkov[1], Peter J. Chockley[3,6], Lourdes Asenath Jimenez Madrigal[1], Giedre Krenciute[3] & Maksim Mamonkin[1,5,7]

Heterogeneity in antigen expression on cancer cells limits clinical benefit of engineered T-cell therapies and underpins treatment resistance through antigen escape. Here, we present a strategy to improve recognition and lysis of tumors with suboptimal antigen expression through a separate engineered receptor that selectively boosts cytotoxic signaling and immune synapse formation. This synapse-stabilizing receptor (SSR) harbors a modified linker for activation of T cells (LAT) endodomain that amplifies CD3ζ signaling upon binding to a secondary tumor antigen resulting in an augmented Ca2+ flux, activation of MAPK and NF-kB signaling, maturation of immune synapse, and enhanced T-cell degranulation. Removing C-terminal amino acids 178-233 in the LAT endodomain (LAT177) was necessary to minimize SSR-mediated cytotoxicity. In models of acute myeloid leukemia, we show that a CD38-targeting SSR boosts cytolysis of antigen-low cancer cells via a C-type lectin-like molecule-1 (CLL1)-specific chimeric antigen receptor (CAR) and a survivin-specific T cell receptor (TCR). Unlike another CAR, SSR does not produce significant cytotoxicity against normal CD38+ tissues. Our study thus shows that SSR arming enhances targeting of antigenically heterogeneous cancers without compromising safety and selectivity of therapeutic T cells.

Chimeric antigen receptor (CAR) T cells can effectively target cancers with high and uniform antigen expression and produce immense clinical benefit in patients with lymphoid malignancies. Other cancers, including acute myeloid leukemia (AML) and many solid tumors, remain resistant to CAR T-cell therapy, in part due to the lack of "safe" tumor-specific target antigens and high heterogeneity of their expression on cancer cells[1–3]. Unlike T-cell receptors (TCRs), which require only several peptide-MHC molecules to trigger T-cell activation, CARs must engage a large number of target antigen molecules on the cell surface to initiate sufficient signaling[4]. This reduced sensitivity of CARs can help minimize damage to normal tissues that express the target antigen at a low level; however, it also underpins a major mechanism of cancer evasion from the adoptive cell therapy where partial antigen downregulation on tumor cells is sufficient to confer

[1]Center for Cell and Gene Therapy, Baylor College of Medicine, Houston, TX, USA. [2]Department of Molecular and Cellular Biology, Baylor College of Medicine, Houston, TX, USA. [3]Department of Bone Marrow Transplantation and Cellular Therapy, St. Jude Children's Research Hospital, Memphis, TN, USA. [4]St. Jude Graduate School of Biomedical Sciences, Memphis, TN, USA. [5]Department of Pathology and Immunology, Baylor College of Medicine, Houston, TX, USA. [6]Present address: The Molecular Medicine and Therapeutics Department, The Ohio State University College of Medicine, Columbus, OH, USA. [7]Present address: Columbia Initiative in Cell Therapy and Engineering, Department of Pediatrics, Columbia University, New York, NY, USA.
e-mail: mm6947@cumc.columbia.edu

resistance to CAR T cells[5,6]. Similarly, downregulation of surface HLA levels has been associated with tumor relapse following allogeneic stem cell transplants and TCR T-cell therapy[7]. Combinatorial antigen targeting using several cytotoxic receptors (or a single receptor with two or more antigen binding domains) has been devised to overcome single antigen escape[8,9]. However, this approach must be developed with caution as multi-antigen targeting can broaden off-tumor toxicities and thus require additional mitigation strategies to prevent unwanted long-term T-cell activity[10].

TCR- and CAR-embedded CD3z chains elicit similar signaling pathways, where Lck-phosphorylated ITAMs on the CD3z molecule recruit ZAP-70 kinase which, upon activation, phosphorylates linker for activation of T cells (LAT)[4]. LAT serves as a main scaffold for the recruitment of phospholipase C gamma 1 (PLC-γ1) and other adapter molecules that propagate downstream signaling cascades and remodeling cytoskeleton to facilitate formation of a cytotoxic immune synapse[11–13]. Therefore, LAT serves as both a key intermediate and an amplifier of CD3ζ signaling thus directly regulating antigen receptor sensitivity.

Here, we hypothesize T-cell activation and cytolysis of antigen-low cancer cells can be augmented by recruiting LAT to CAR or TCR. We surmise this non-cytotoxic synapse-stabilizing receptor (SSR) does not trigger T-cell activation per se but instead amplify CD3ζ signaling from the main antigen receptor thus improving T-cell degranulation and target cell killing. To that end, we engineer LAT-based receptors harboring an extracellular domain targeting CD38 – a surface antigen abundantly expressed in leukemia as well as in critical normal blood cells and primitive progenitors. In this report, we use preclinical models of AML to show a CD38-specific SSR arming improves CAR- and TCR-mediated cytolysis of antigen-low leukemia without producing additional toxicity against healthy CD38+ tissues. Our results suggest this modification can be applied broadly to other antigens and disease settings to improve antigen sensitivity of therapeutic T cells.

Results

CD38.SSR harboring a LAT177 endodomain improved antigen-specific cytolysis of AML by C-type lectin-like molecule-1 (CLL1).CAR T cells

To test the concept of LAT-mediated potentiation of CAR signaling, we created a prototypic synapse-stabilizing receptor (SSR) using a CD38-specific binder connected via a CD8a spacer and transmembrane region to the endodomain of linker for activated T cells (LAT). We co-expressed the CD38.SSR with a second-generation, CD28-costimulated CAR targeting CLL-1 (Fig. 1A), a myeloid antigen commonly expressed in AML at various levels. As both the CAR and the SSR utilize a CD8a spacer, we introduced the Cys164Ser mutation in the SSR spacer, abrogating covalent heterodimerization of the two receptors via a cysteine bond[14]. Further, full-length LAT endodomain (LATFL) has been shown to spontaneously oligomerize with SLP-76 via GADS/Grb2 adapter molecules[13,15,16], producing spontaneous T cell activation which may be exacerbated by the expression of the SSR ligand CD38 on activated T cells[17]. Therefore, we created an additional SSR variant with a truncated LAT endodomain (LAT177) that retains PLC-γ1 binding via Tyr132 but lacks Tyr191 and Tyr226 residues required for GADS/Grb2 docking and SLP-76 oligomerization (Fig. 1A). CD38.SSRs harboring either LATFL and LAT177 endodomain were expressed at high levels with CLL1.CAR on T cells via gammaretroviral co-transduction routinely resulting in co-expression on >85% of T cells (Fig. 1B). Co-expression of SSR-LATFL and CLL1.CAR significantly reduced the expansion of dual-transduced T cells (Supplementary Fig. 1A), possibly reflecting excessive tonic CAR signaling amplified by the full-length LAT as T cells expressing SSR-LATFL alone demonstrated normal expansion (Supplementary Fig. 1A). In contrast, LAT177 truncation attenuated this effect and improved the expansion of SSR-armed CLL1.CAR T cells (Supplementary Fig. 1A). Unlike LATFL, LAT177-harboring CD38.SSR had minimal effect on the differentiation status and subset composition of expanded T cells (Supplementary Fig. 1B). Notably, T cells expressing SSR-LATFL alone produced significant cytotoxicity against CD38+ target cell lines Molm13 and CCRF-CEM indicating activation of cytotoxic signaling upon engaging the full-length LAT endodomain thus acting as a "weak CAR" (Fig. 1C). In contrast, T cells expressing SSR-LAT177 had minimal activity against the same target cells (Fig. 1C) suggesting LAT truncation is required to minimize background cytotoxicity of the SSR. Given the "leakiness" of the full LAT endodomain in the CD38.SSR and cellular toxicity induced by its expression in T cells, we opted to utilize the CD38.SSR construct with the truncated LAT177 endodomain for subsequent analyses.

Next, we evaluated the activity of CD38.SSR in CLL1.CAR T cells targeting cancer cells with low antigen expression and compared it with other CD38-specific chimeric costimulatory receptors and a full-length cytotoxic CD38.CAR. We generated T cells expressing CLL1.CAR alone or in combination with a truncated (ΔSSR) construct or an SSR harboring either a TNFR superfamily endodomain (4-1BB or CD27), or an immunoglobulin superfamily endodomain (CD28), or a LAT177 endodomain, via gammaretroviral co-transduction. We also created a cytotoxic second-generation CD38.CAR (where the LAT endodomain was replaced with CD28 and CD3ζ signaling domains) as a control (Supplementary Fig. 2A). The expansion of SSR.LAT177-expressing T cells was comparable with those expressing a control truncated SSR lacking signaling endodomain (ΔSSR) or with T cells expressing SSR with a CD28 endodomain (Supplementary Fig. 2B–D). In contrast, expansion of T cells expressing SSRs with CD27 or 4-1BB endodomain was significantly impaired (Supplementary Fig. 2B–E). We have previously shown constitutive (tonic) TRAF2-NFkB signaling from chimeric TNFRSF endodomains produced cellular toxicity in T cells transduced with a gammaretroviral vector which is consistent with this observation[18,19]. Expectedly, the expansion of CLL1.CAR T cells co-expressing a full length CD38.CAR was also reduced, reflecting a CD38-directed T-cell fratricide[20].

CLL1 expression in primary AML is very heterogeneous, ranging from dim/negative to bright, often within the same patient[21,22]. An AML line THP-1 represents the latter scenario whereas Molm13 AML cells express low levels of CLL1 insufficient for effective recognition and cytolysis by CLL1.CAR T cells[22,23] (Fig. 1D). Both lines expressed CD38 on the cell surface (Fig. 1D). As expected, CLL1.CAR T cells displayed minimal activity against Molm13 cells (Fig. 1E). The cytotoxicity of CLL1.CAR T cell against Molm13 was only marginally improved by co-expressing a truncated non-signaling (ΔSSR) or CD27-harboring SSR (Fig. 1E). In contrast, CLL1.CAR T cells armed with CD28- or LAT177-based SSRs or a full cytotoxic CD38.CAR produced significantly greater killing of Molm13 and expansion upon a 3-day co-culture (Fig. 1E). However, CAR T cells expressing a CD28-based SSR also killed CCRF-CEM cells which do not express CLL1, reflecting unwanted CD38-driven activation that is independent of the CLL1.CAR (Fig. 1E). Co-expression of ΔSSR or SSR-LAT177 resulted in a reduced but still detectable cytotoxicity against control CCRF-CEM cells (Fig. 1E). This low-level cytotoxicity was further attenuated by either knocking out the CD3ε gene on T cells or removing MHC I on CCRF-CEM using CRISPR/Cas9, suggesting CD38 binding by SSR amplified allogeneic killing of mismatched cancer cells (Supplementary Fig. 3A–C). In contrast, CLL1 CAR T cells co-expressing SSR.CD28 displayed significant cytotoxicity against CCRF-CEM even after the knock-out of CD3ε or β2m indicating TCR/MHC-independent killing. CD3 editing did not attenuate killing of Molm13 by CAR.SSR T cells indicating CAR-mediated cytotoxicity (Supplementary Fig. 3D). Further, SSR co-expression improved killing of THP-1 AML but not KG1a, which expresses lower levels of CLL1 and CD38 (Supplementary Fig. 4A–C). CLL1.CAR T cells armed with either SSR-LATFL or SSR-LAT177 produced comparable improvement in killing Molm13 and CAR T-cell expansion (Supplementary Fig. 4D).

https://doi.org/10.1038/s41467-025-65897-4

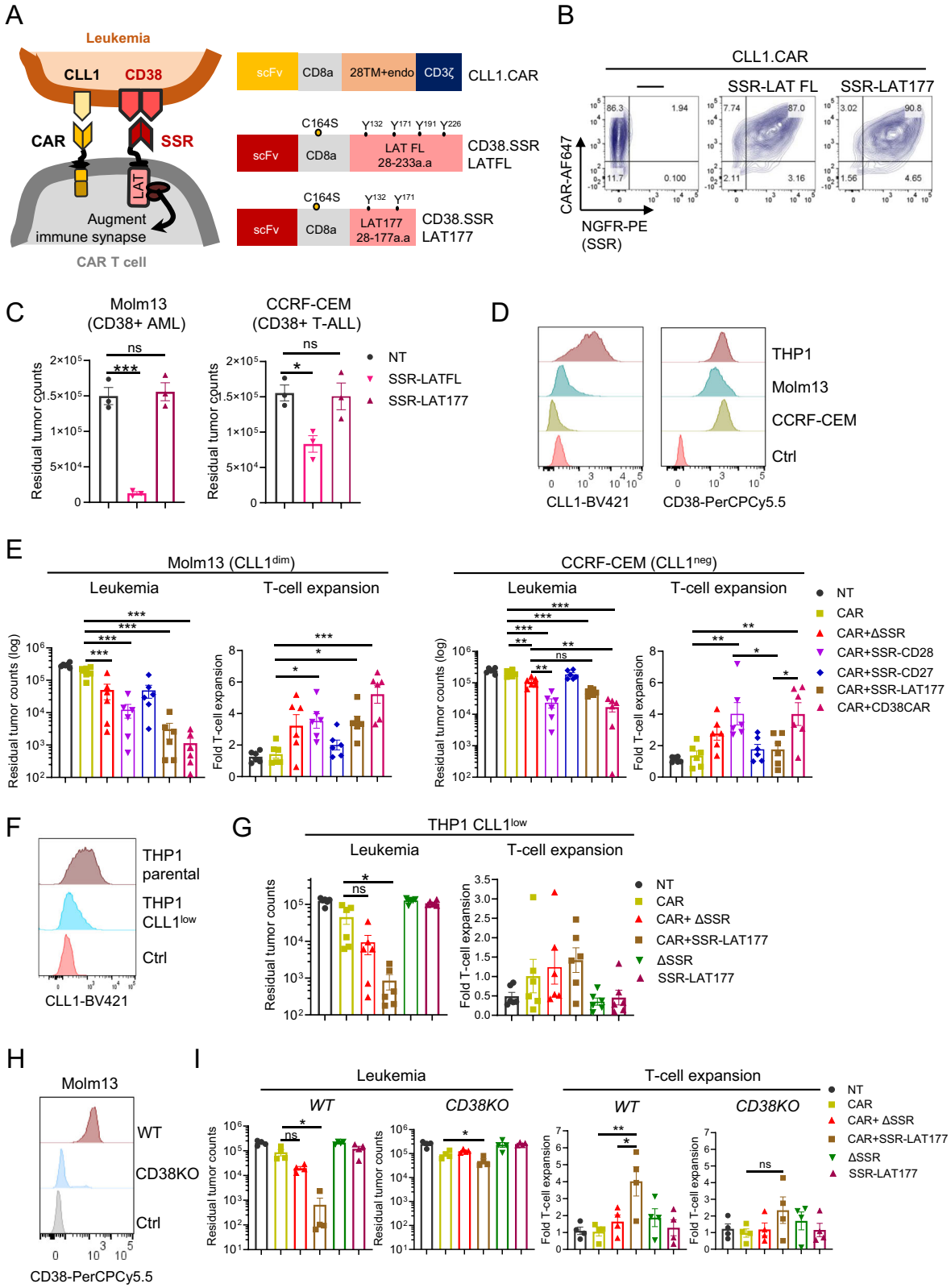

To further validate the potency of SSR in CAR sensitivity, we co-cultured CLL1.CAR.SSR T cells with a CLL1^{low} derivative of THP1 cells obtained by sort-purifying THP1 cells expressing dim levels of CLL1 (Fig. 1F). Consistent with the results obtained with Molm13, expression of CD38.SSR significantly improved cytotoxicity of CLL1.CAR T cells against THP1 CLL1^{low} cells, whereas unarmed CAR T cells showed only limited activity (Fig. 1G). Engaging CD38 on target cells is critical for the CD38.SSR activity as genetic ablation of the CD38 gene on Molm13 reduced the benefit of the SSR on CAR T-cell cytotoxicity and expansion during co-culture, suggesting SSR.LAT177-mediated augmentation of CLL1.CAR-mediated cytotoxicity was largely dependent on CD38 expression (Fig. 1H, I). SSR.LAT177 co-expression enhanced cytotoxicity and expansion of T cells expressing other CLL1.CAR constructs, including a CD28-costimulated CAR with a CD28 hinge and a

Fig. 1 | CD38-specific synapse stabilizing receptor (SSR) harbouring a truncated LAT endodomain improves CLL1.CAR-mediated killing of antigen-low AML. A A schematic showing interaction between CLL1.CAR and CD38.SSR. CAR and SSR configurations are denoted on the right **B** Representative flow plots showing co-expression of CAR and SSRs on day7 post co-transduction (TD). SSR expression was measured by detection of a surrogate maker truncated NGFR. **C** Residual tumor counts after a 3-day culture of CD38+ Molm13 (AML) and CCRF-CEM (T-ALL) with non-transduced T cells (NT) or SSR T cells at an E:T ratio 1:4. Data represent 3 donors. *P* values were determined using one way ANOVA with Tukey's correction for multiple comparisons. Bar graphs show mean+S.E.M. (*$P < 0.05$, **$P < 0.01$, ***$P < 0.001$. ns, non-significant). **D** Histograms showing CLL1 and CD38 levels in indicated cell lines. **E** Residual tumor counts and T-cell expansion after a 3-day co-culture of Molm13 and CCRF-CEM with CAR T cells at a E:T ratio 1:4. Data represent 6 donors from 3 independent experiments. *P* values were determined using one way ANOVA with Tukey's correction for multiple comparisons. Bar graphs show mean + S.E.M. (*$P < 0.05$, **$P < 0.01$, ***$P < 0.001$. ns, non-significant). **F** Histograms showing CLL1 and CD38 levels in pre-sorted THP1 and CLL1-low THP1 post-sorting. **G** Residual tumor counts and fold T-cell expansion after 3 day culture at a E:T ratio 1:4. Data represent 6 donors from 2 independent experiments. *P* values were determined using one way ANOVA with Tukey's correction for multiple comparisons. Bar graphs show mean + S.E.M. (*P < 0.05. ns, non-significant). **H** CD38 expression in the parental and knock-out line of Molm13. **I** Residual tumor counts and fold T-cell expansion after 3 day culture at a E:T ratio 1:4. Data represent 4 donors from 2 independent experiments. *P* values were determined using one way ANOVA with Tukey's correction for multiple comparisons. Bar graphs show mean + S.E.M. (*$P < 0.05$, **$P < 0.01$, ***$P < 0.001$. ns, non-significant). (*$P < 0.05$, **$P < 0.01$. ns, non-significant).

4-1BB costimulated CAR (Supplementary Fig. 5), suggesting the SSR is not sensitive to a CAR configuration or a choice of costimulation. These results indicate CD38.SSR with a LAT177 endodomain produced the highest augmentation of CAR T cell-mediated killing of CLL1-low AML without compromising CAR specificity.

CD38.SSR enhanced effector function and immune synapse formation of CAR-T cells

LAT is a scaffolding molecule that orchestrates TCR signal transmission by the Lck-activated ZAP70 kinase to the key downstream kinase PLCγ1 which directly binds to Tyr132 that is retained in the LAT177 endodomain. PLCγ1 promotes cleavage of PIP2 to diacyl glycerol (DAG) and IP3 resulting in Ca^{++} influx and activation of MAPK and NF-κB pathways triggering T-cell effector program. The live cell imaging revealed SSR co-expression improved Ca^{++} influx in CAR T cells upon a 30-min co-culture with Molm13 target cells compared to control unarmed CAR T cells (Fig. 2A, B). Intriguingly, the increase in calcium levels was also observed in T-cells expressing ΔSSR or SSR alone (Supplementary Fig. 6A), suggesting this effect is secondary to the SSR-mediated engagement of CD38 which mediates intracellular Ca++ release via NAADP signaling[24–26].

Next, we evaluated activation of PLCγ and its downstream signaling in SSR-armed CLL1 CAR T cells stimulated with plate-bound recombinant CLL1 and CD38. We observed higher levels of PLCγ1 phosphorylation and the downstream MAPK (ERK1/2) and NF-kB pathways in SSR-expressing CAR T cells compared to control CAR T cells (Fig. 2C, D). Engagement of the SSR alone did not activate the PLCγ1 pathways in the absence of CAR signaling (Supplementary Fig. 6B, C). Mutation of the PLCγ1 binding site Y132 in the LAT177 endodomain minimized SSR activity upon coculture with Molm13, highlight the critical role of PLCγ1 in SSR.LAT177 function (Fig. 2E, F).

Next, we assessed how SSR affects the formation of CAR-mediated cytotoxic immune synapse using super-resolution confocal imaging of CLL1.CAR T cells exposed to Molm13 cells for 1 h. While observing limited enhancement of lytic granule migration by SSR (Supplementary Fig. 7A, B), co-expression of SSR in CLL1.CAR T cells significantly improved polarization of filamentous actin (F-Actin) and the microtubule organizing center (MTOC) to the immune synapse, reflecting cytoskeleton reorganization and the formation of a more stable synapse (Fig. 3A). We also observed a trend towards enhanced recruitment of phospho-SLP76, a critical signaling partner of LAT (Fig. 3A, B). Expression of the SSR.LAT177 alone did not significantly affect polarization of the synaptic machinery (Fig. 3A, B), suggesting increased Ca^{++} influx was insufficient to trigger effector function of SSR-LAT177 expressing T cells in the absence of CAR signaling, consistent with prior findings.

In line with the augmentation of signaling and immune synapse formation, we found SSR co-expression on CLL1.CAR T cells increased intracellular production of IFN-γ in both $CD4^+$ and $CD8^+$ T cells and augmented IL-2 production by CD4 + T cells upon a 4-h co-culture with $CLL1^{low}$ Molm13 cells (Fig. 3C and Supplementary Fig. 7C). We also observed higher production of granzyme B and degranulation, as measured by surface CD107a, in both $CD4^+$ and $CD8^+$ T cells suggesting SSR activity amplified the cytolytic program in $CD4^+$ T cells (Fig. 3D). Of note, co-expression of a truncated SSR lacking the LAT177 endodomain (ΔSSR) had minimal effect on cytokine production and degranulation highlighting the active role of the LAT endodomain in potentiating CAR-mediated cytotoxicity.

To evaluate whether the SSR.LAT177-mediated enhancement of CAR cytotoxicity is a general phenomenon, we designed an SSR targeting GRP78, a protein upregulated on the cell surface of several tumors, including gliomas[27]. We co-expressed GRP78.SSR with a CAR targeting IL13Ra2[28], an antigen expressed in diffuse intrinsic pontine gliomas (DIPG) at varying levels (Supplementary Fig. 8A-C). GRP78.SSR improved the killing of two tumor cell lines derived from patients with DIPG and enhanced intracellular Ca + + flux in IL13Ra2 CAR T cells (Supplementary Fig. 8D, E). In contrast to the CD38.SSR, GRP78.SSR did not produce spontaneous Ca + + flux in CAR-negative T cells.

Collectively, these results indicate SSR expression promotes the formation of a mature cytotoxic immune synapse between a CAR T cell and a target cell with low antigen expression, thus potentiating intracellular signaling and promoting cytokine production and degranulation.

SSR co-expression boosts anti-leukemic activity of CAR T cells in vivo

To evaluate the effect of SSR on CAR T-cell mediated tumor control in vivo, we utilized two mouse xenograft models of human AML. In the first model, we engrafted Molm13 cells into NSG mice lacking murine MHC Class I and Class II genes to reduce non-specific xenoreactivity by human T cells (NSG-MHCKO). Three days following AML injection, we injected a single dose of control non-transduced T cells or T cells expressing CLL1.CAR alone or in combination with CD38.SSR (Fig. 4A). Bioluminescence imaging of AML burden showed only minimal disease control by control unarmed CLL1.CAR T cells, whereas SSR.LAT177-coexpressing CAR T cells suppressed systemic expansion of leukemia and produced better expansion in peripheral blood in the first 10 days post-infusion, significantly extending the survival of animals (Fig. 4B–E). Of note, co-expression of a non-signaling ΔSSR did not enhance anti-tumor activity and expansion of CLL1 CAR T cells in vivo, suggesting LAT177 signaling is critical for the optimal SSR function in vivo (Fig. 4B–D). SSR-armed CLL1.CAR T cells had a higher frequency of CD62L + CD45RA+ naïve-like T cells 18 days post-infusion compared to unarmed CLL1.CAR T cells (Supplementary Fig. 9).

To validate these findings in another model of AML with suboptimal target antigen expression, we modified $CLL1^{low}$ THP-1 cells to express firefly luciferase and engrafted into NSG-MHCKO mice followed by a single injection of CAR T cells (Fig. 4F). Again, CLL1.CAR T cells demonstrated poor activity against the antigen-low leukemia, and non-transduced or SSR-only T cells had minimal, if any, effect on

https://doi.org/10.1038/s41467-025-65897-4

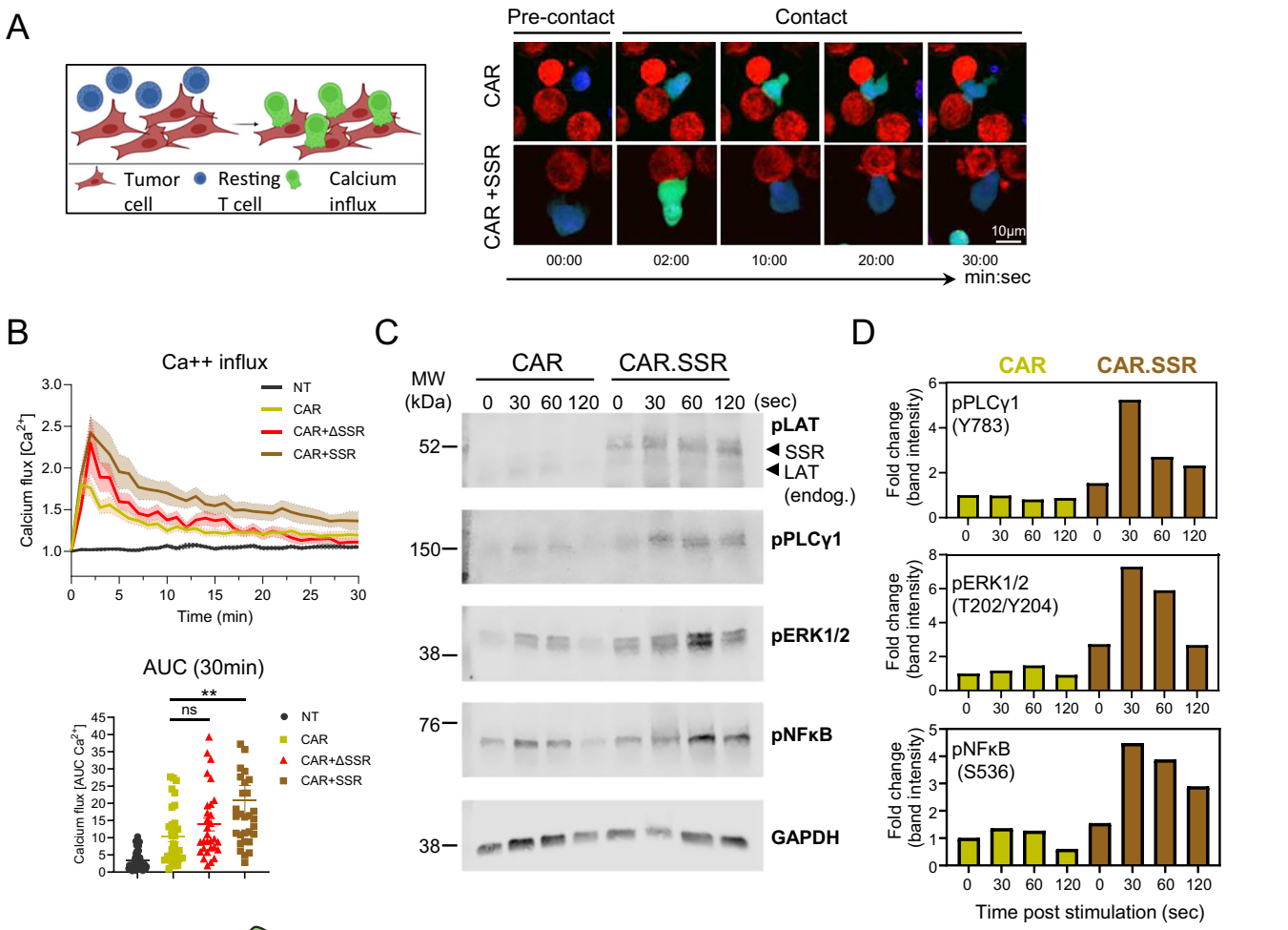

Fig. 2 | CD38.SSR augmented activation signaling in CAR T cells. A Schematic illustration (left) and representative images (right) of calcium influx (green) in T cells (blue) at pre-contact or post-contact with Molm13 (red) over the indicated time course. **B** Calcium (Ca++) flux in T cells interacting with Molm13 over the indicated timepoints, and the mean area under the curve (AUC) for the initial 30 min post-contact. Each dot represents a single cell. Data include single cells (42 cells (NT), 34 cells (CAR), 30 cells (CAR + ΔSSR), 30 cells (CAR + SSR)) combined from 3 independent donors and experiments. *P* values were determined using one way ANOVA with Tukey's correction for multiple comparisons. Dot plots show mean + S.E.M. (*$P < 0.05$, **$P < 0.01$, ns, non-significant). **C** Western blots showing the detection of phospho-proteins and GAPDH harvested from CAR or CAR.SSR T cells stimulated with plate-coated anti-CLL1 CAR antibody and recombinant CD38 at indicated time points. Data were repeated in three independent experiments using 3 donors. MW, molecular weight. **D** Densitometry analysis of pPLCγ1, pERK1/2 and pNF-KB normalized to GAPDH. **E** Schematic of an SSR construct containing a point mutation Y132F in the LAT endo-domain, and flow plots (bottom) showing the co-expression of CAR and SSR or SSR with Y132F on day 6 post transduction. **F** Residual tumor counts (left) and T-cell expansion normalized to day 0 (right) in a 3 day co-culture with Molm13. Data represent two independent experiments with 4 donors. *P* values were determined using one way ANOVA with Tukey's correction for multiple comparisons. Bar graphs show mean + S.E.M. (*$P < 0.05$, ns, non-significant).

https://doi.org/10.1038/s41467-025-65897-4

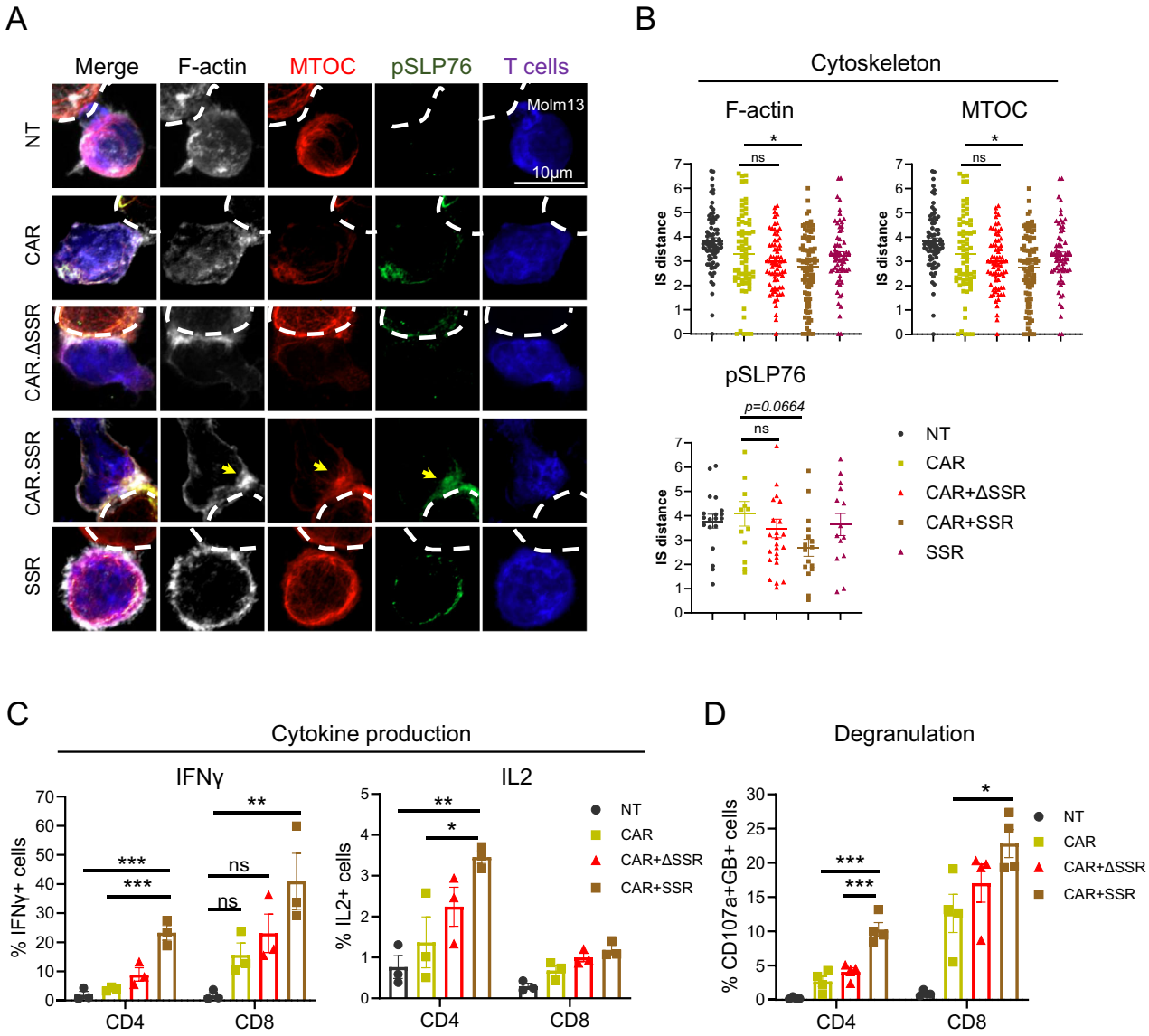

Fig. 3 | CD38.SSR enhanced effector function and immune synapse polarization of CAR T cells upon co-culture with antigen-low AML. A Representative fluorescence confocal microscopy of F-actin and microtubule organizing center (MTOC) as well as pSLP76 after 1 h of co-culture of CLL1.CAR T cells with Molm13. White bars denote 10 μm. **B** Quantitative single-cell analysis of the distance from F-actin, MTOC and pSLP76 to the immune synapse. Each dot represents a single cell derived from either 4 donors (F-actin, 77 cells (NT), 70 cells (CAR), 73 cells (CAR + ΔSSR), 92 cells (CAR + SSR) and 64 cells (SSR), and MTOC, 67 cells (NT), 56 (CAR), 65 (CAR + ΔSSR), 76 (CAR + SSR), 52 cells (SSR)) or 3 donors (pSLP76, 19 cells (NT), 13 cells (CAR), 25 cells (CAR + ΔSSR), 16 cells (CAR + SSR) and 14 cells (SSR)) independent donors respectively. *P* values were determined using one way ANOVA with Dunnet's correction for multiple comparisons compared to CAR. Dot plots show mean + S.E.M. (*$P < 0.05$, **$P < 0.01$. ns, non-significant). **C** Percentages of IFNγ and IL-2 positive or (**D**) GzB/CD107a double positive cells in CD4+ and CD8+ subsets of CLL1.CAR T cells after a 4-h co-culture with Molm13 at 1:1 E:T ratio. Data represent 3–4 donors. *P* values were determined using one way ANOVA with Tukey's correction for multiple comparisons. Bar graphs show mean + S.E.M. (*$P < 0.05$, **$P < 0.01$, ***$P < 0.001$. ns, non-significant).

tumor growth (Fig. 4G, H). By contrast, SSR-armed CLL1.CAR T cells controlled systemic leukemia in most animals, resulting in their long-term survival (Fig. 4I). SSR-armed CLL1.CAR T cells had reduced frequency of PD1 + LAG3+ cells compared to unarmed CAR T cells on day 61 post-infusion (Supplementary Fig. 10) possibly reflecting reduced systemic tumor burden. These results indicate SSR expression significantly boosts anti-leukemic activity of CLL1.CAR T cells against antigen-low AML in vivo.

Co-targeting CD38 through SSR enhances CAR-T targeting of primary AML but not healthy cells

For optimal activity, SSR must selectively improve CAR T-cell cytotoxicity against cancerous cells that express both CAR and SSR antigens without producing additional cytotoxicity against normal tissues that express the SSR target antigen. Among mature circulating cells, CD38 was expressed at the highest levels on $CLL1^+$ monocytes and $CLL1^-$ NK cells and varying levels on T- and B-cells (Fig. 5A and Supplementary Fig. 11A-B). Co-expression of the CD38.SSR did not enhance cytotoxicity of CLL1.CAR T cells against autologous monocytes and produced no activity against CLL1-negative autologous T cells and B-cells (Fig. 5B). A weak activity of SSR-armed CLL1.CAR T cells was detected against CD38 bright NK cells, but it did not reach statistical significance, unlike in control CD38.CAR T cells (Fig. 5B, C and Supplementary Fig. 11C). T cells expressing SSR alone had no measurable activity against autologous lymphocytes but produced weak cytotoxicity against HLA-

https://doi.org/10.1038/s41467-025-65897-4

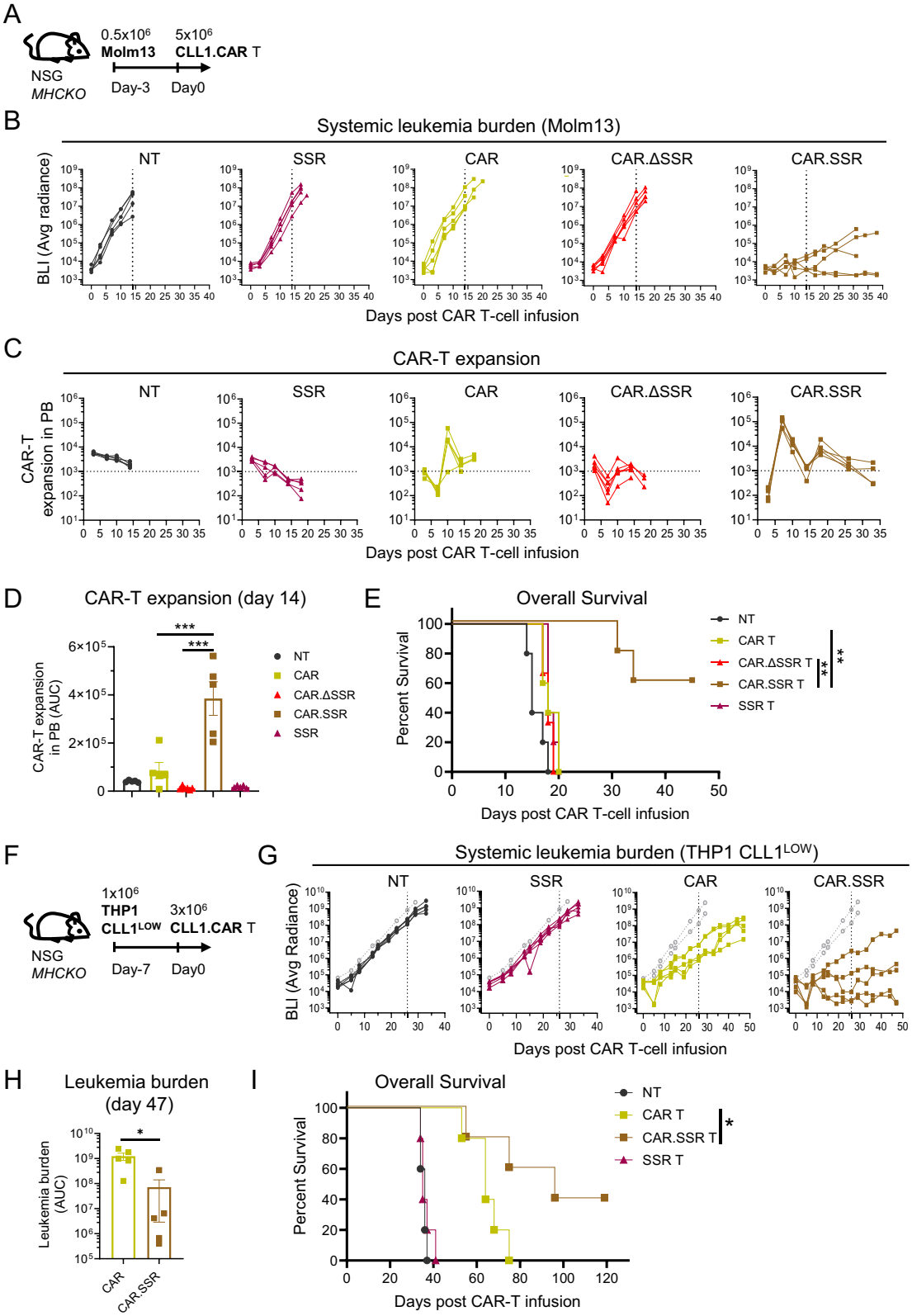

Fig. 4 | CLL1.CAR T cells armed with CD38.SSR suppressed progression of systemic leukemia and prolonged animal survival. A Schematic of the Molm3 AML model. **B** Systemic leukemia progression monitored by bioluminescence (BLI) and (**C**) CAR T-cell counts (hCD45 + hCD3+CAR+) in peripheral blood were tracked at indicated days post CAR T-cell infusion. **D** AUC of CAR-T expansion between day 0 and day 14. *P* values were determined using one way ANOVA with Tukey's correction for multiple comparisons. Bar graphs show mean + S.E.M. (***$P < 0.001$). **E** Overall mouse survival in the Molm13 AML model with 5 mice for each group. Statistical significance was determined by a log rank test for the survival curve. Statistical significance was determined by a log rank test for the survival curve. (**$P < 0.01$). **F** Schematic timeline of the THP1-CLL1^{LOW} model. **G** Systemic leukemia progression monitored by bioluminescence imaging (BLI). **H** AUC of leukemia burden from day 0 to day 47. The data include 5 mice for each group. P values were determined by a two-tailed unpaired Student's t test. Bar graphs show mean + S.E.M. (*$P < 0.05$). **I** Overall mouse survival in the THP1-CLLlow model ($n = 5$ mice per each group). Statistical significance was determined by a log-rank test. (*$P = 0.0487$).

mismatched CD38-high T-ALL cell lines P12-ICHIKAWA and CCRF-CEM (Supplementary Fig. 11D, E).

In addition to mature blood cells, CD38 is expressed in primitive hematopoietic progenitors where its expression decreases at later stages of myeloid differentiation as CLL1 expression increases inversely[3,29,30]. To assess the activity of CD38.SSR-armed CLL1.CAR T cells against hematopoietic progenitors, we purified CD34+ cells from cord blood (Fig. 5C) and co-cultured them with control non-transduced or armed and unarmed CLL1.CAR T cells for 5 h at an effector-to-target ratio of 10:1 followed by a 12-day culture on a semi-solid methylcellulose medium supportive of myeloid differentiation. We saw no activity of CLL1.CAR T cells with or without SSR against CLL1-negative erythroid progenitors (BFU-E, Fig. 5C). While granulocytic/monocytic progenitors (CLL1+) were expectedly targeted by CLL1.CAR T cells, addition of the SSR did not increase that cytotoxicity (CFU-GM, Fig. 5C). By contrast, co-expression of a cytotoxic CD38.CAR produced ablation of both types of CD38+ progenitors (Fig. 5C). Therefore, CD38.SSR does not exacerbate toxicity of CAR T cells against normal CD38+ tissues.

To evaluate the benefit of SSR in targeting primary AML, we co-cultured T cells with leukemic blasts obtained from two patients with treatment-refractory AML expressing CD38 and varying levels of CLL1 (Fig. 5D). SSR-armed CLL1 CAR T cells produced a significantly better killing of AML blasts from both patients, comparable with dual-CAR T cells (Fig. 5E). Therefore, SSR enhances killing of malignant blasts but not healthy CD38+ tissue.

CD38 SSR improved anti-tumor function of TCR-expressing T cells

Antigen heterogeneity does not affect only CAR T cells as tumor cells also commonly downregulate surface HLA molecules to evade TCR-mediated recognition. To assess the utility of SSR in potentiating TCR-mediated lysis of leukemia with low HLA expression, we tested its activity in T cells expressing a TCR targeting intracellular protein survivin/BIRC5 presented on HLA-A2 (Fig. 6A)[31]. SSR was co-expressed in Survivin TCR (Sur-TCR) T cells at high levels without affecting the expansion and subset composition of transgenic T cells derived from both HLA-A2- and HLA-A2+ donors indicating SSR expression does not enhance fratricide of Sur-TCR T cells which upregulate survivin during activation[31] (Fig. 6B, C and Supplementary Fig. 12A–C). We postulated this is because SSR masks CD38 in T cells *in cis* thus preventing its recognition by the surrounding SSR T cells. Indeed, we observed complete loss of detectable surface CD38 in SSR-expressing T cells by flow cytometry utilizing an antibody binding to an epitope that overlaps with the SSR CD38 binder, supporting cis-masking (Supplementary Fig. 13A, B). To further test this hypothesis, we incubated control and SSR-armed CAR T cells with a cytotoxic CD38-specific monoclonal antibody daratumumab in the presence of purified NK cells. Expression of CD38.SSR prevented daratumumab-induced NK cell-mediated cell cytotoxicity to T cells illustrating protective masking of surface CD38 by the SSR (Supplementary Fig. 13C, D).

Next, we utilized three HLA-A2+ acute leukemia lines with a similar expression level of survivin but varying levels of surface HLA-A2, ranging from high in BV173 to intermediate in THP1 to low in TALL1 (Fig. 6D). While Sur-TCR T cells produced cytotoxicity against HLA-high BV173 cells, SSR co-expression further improved T-cell expansion in a 3 day co-culture (Fig. 6E and Supplementary Fig. 12D). We observed no cytotoxicity of unarmed Sur-TCR T cells against THP1 cells that express intermediate levels of HLA on the cell surface. However, SSR co-expression produced significant cytotoxicity against THP1 cells but did not improve T-cell expansion (Fig. 6E and Supplementary Fig. 12D). Finally, Sur-TCR T cells produced no killing of HLA-low cell line TALL1, regardless of the SSR co-expression, indicating the benefit of the SSR is limited to a dynamic range of main antigen expression. SSR-armed Sur-TCR T cells produced higher degranulation upon a short co-culture with BV173 and THP1 cells, and improved cytokine production upon co-culture with THP1 (Fig. 6F, G), consistent with observations in CAR T cells.

Next, we assessed whether SSR can improve the anti-tumor activity of Sur-TCR T cells in vivo using THP-1 cells resistant to Sur-TCR cytotoxicity. We established systemic THP1 leukemia via intravenous injection in NSG-MHCKO mice for 7 days and administered three doses of Sur-TCR T cells in the next week. Mice received IP injections of 2000 IU of exogenous rhIL2 twice a week for three weeks (Supplementary Fig. 14A). While unarmed Sur-TCR T cells had no significant activity against systemic leukemia compared to control (tumor only) condition, SSR-armed Sur-TCR T cells delayed leukemia progression and reduced levels of circulating AML blasts in peripheral blood (Supplementary Fig. 14B, C) significantly extending overall animal survival (Supplementary Fig. 14D). The activity of Sur-TCR T cells was transient and the SSR benefit limited (Supplementary Fig. 14D), likely due to the lack of critical Signals 2 and 3 that are required to maintain functional persistence of therapeutic T cells in a mouse. To further improve the in vivo efficacy, we modified Sur-TCR T cells to express membrane-bound IL15 thus providing continuous Signal 3[32–34] (Supplementary Fig. 15A–D). Mice were engrafted with THP-1 cells followed by a single injection of Sur-TCR T cells armed with ΔSSR or SSR (Fig. 6H). The cytokine modification slightly increased their persistence and anti-tumor activity of sur-TCR T cells (Supplementary Fig. 15E), and SSR co-expression enabled stronger anti-tumor control significantly prolonging animal survival (Fig. 6I–K). Consistent to CAR.SSR T cells, SSR-armed survivin T cells displayed a higher frequency of CD62L + CD45RA+ naïve-like T cells 27 days post-infusion compared to TCR.ΔSSR and unarmed TCR T cells (Supplementary Fig. 15F).

Taken together, these results demonstrate specific and potent augmentation of CAR- and TCR-mediated cytolysis of tumor cells expressing suboptimal levels of target antigens by a synapse-stabilizing receptor harboring LAT177 endodomain.

Discussion

We show CAR- or TCR-mediated cytolysis of antigen-low cancer cells can be boosted through a non-cytotoxic synapse-stabilizing receptor that amplifies antigen receptor signaling via a modified LAT endodomain. In models of antigenically heterogenous AML, a synapse-stabilizing receptor targeting CD38 improved anti-tumor function of CLL1.CAR- and survivin-specific TCR- T cells without broadening off-tumor toxicity against normal CD38+ tissues. These results support the concept of conditional augmentation of antigen sensitivity of therapeutic T cells through an engineered receptor targeting a secondary antigen.

Several solutions to the problem of antigen modulation in cancer have been proposed to enhance the efficacy of engineered immune effectors. T cells can be modified to express two or more CARs targeting different antigens implementing a Boolean “OR” gate. Similarly, a single tandem CAR can recognize two distinct antigens in the same Boolean logic[10,21]. These strategies help offset the risk of a single antigen escape but require additional considerations for off-tumor toxicity that can be broadened by targeting multiple independent antigens. Alternatively, chimeric costimulatory receptors (CCRs) targeting a secondary antigen and providing heterologous 4-1BB costimulation have been developed to improve targeting of B-cell malignancies with CD28-costimulated CD19 and BCMA CARs[35]. An application of CCRs in AML where CLL1-targeting CCR eliciting 4-1BB costimulation improves the activity of ADGRE2 CAR T cells is another example of Boolean “AND” or “IF-BETTER” gating; this strategy is currently being evaluated in a clinical trial[36]. Expression of CCRs targeting folate receptor and CD19 on T cells augmented TCR-mediated targeting in preclinical models of ovarian cancer and EBV lymphomas, respectively[37,38]. The major distinction between these approaches and the SSR described in this

https://doi.org/10.1038/s41467-025-65897-4

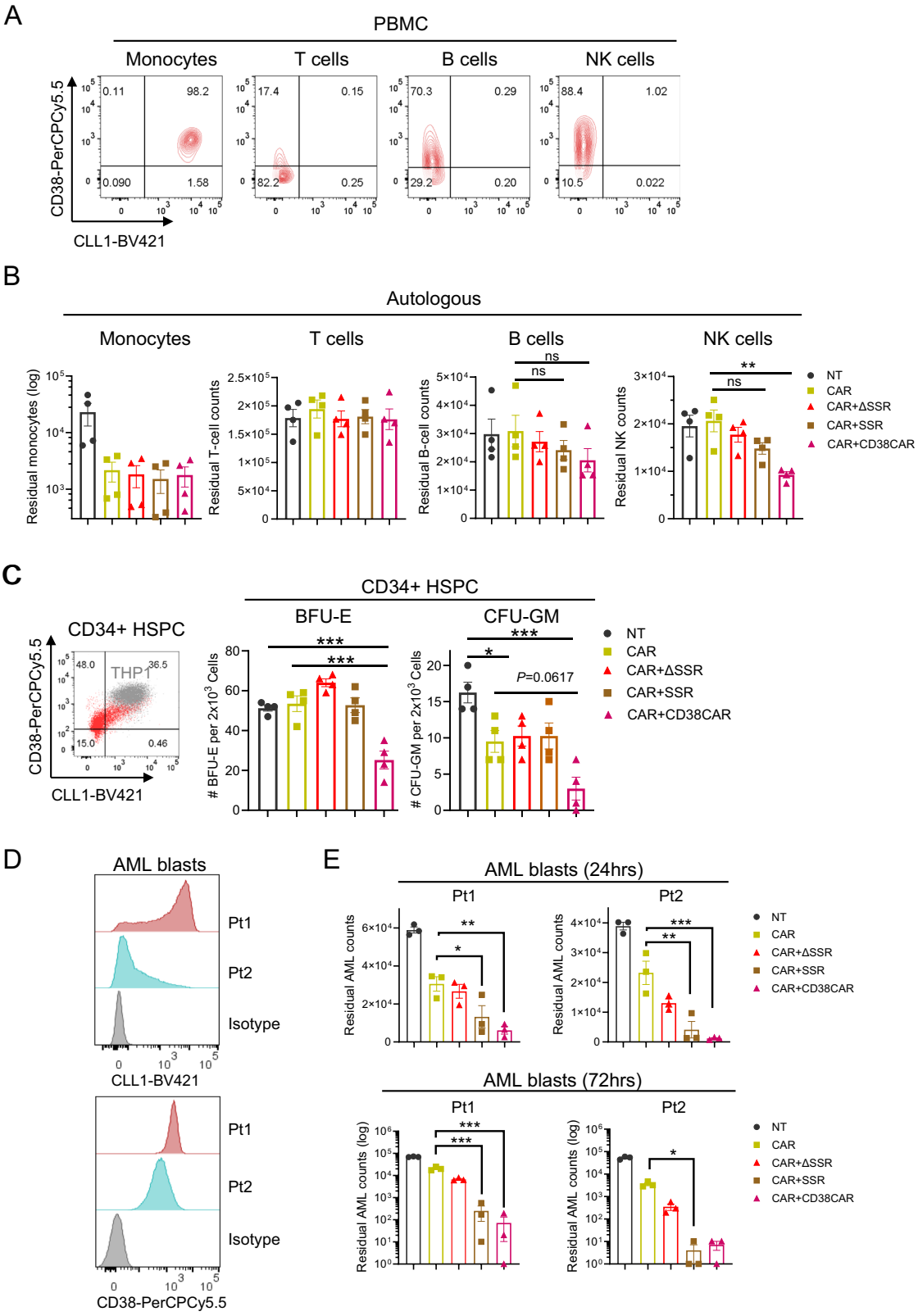

study is that an SSR does not elicit additional Signal 2 from a conventional costimulatory endodomain. Instead, an SSR amplifies CD3z signaling by recruiting additional LAT molecules and boosts downstream signaling that augments a cytotoxic immune synapse. This strategy selectively enables killing tumors with otherwise untargetable levels of antigen expression (Boolean "AND" gate) or improves recognition of antigen-dim cancer cells ("IF-BETTER" gate) without producing significant activity against tissues that lack CAR or TCR antigen.

Passive binding of a secondary antigen by an SSR may stabilize the T cell:target cell contact and increase the avidity of this interaction. Indeed, we observed modest but detectable improvement of MOLM13 leukemia killing in vitro even by CAR T cells armed with a truncated, non-signaling SSR. However, this benefit did not translate to improved

Fig. 5 | SSR produced limited activity against healthy CD38+ leukocytes and hematopoietic progenitors. A Representative flow plots showing expression of CD38 and CLL1 in PBMCs including CD14+ monocytes, CD3 + T cells, CD3-CD56 + NK cells and CD19 + B cells. **B** Residual PBMCs after a 24-h co-culture with autologous T cells at a 1:4 E:T ratio. Data represent 4 donors. *P* values were determined using one way ANOVA with Tukey's correction for multiple comparisons. Bar graphs show mean + S.E.M. (**$P < 0.01$. ns, non-significant). **C** Quantification of a burst forming unit-erythroid (BFU-E) and colony forming unit-granulocyte/macrophage (CFU-GM) from hematopoietic stem cells/progenitors (HSPC) after 5-h co-culture of indicated CAR T cells with CD34+ cord blood cells at a E:T ratio 10:1, and expanded for 12 days in semi-solid methylcellulose. Data represent 4 donors. *P* values were determined using one way ANOVA with Tukey's correction for multiple comparisons. Bar graphs show mean + S.E.M. (*$P < 0.05$, **$P < 0.01$, ***$P < 0.001$. ns, non-significant). **D** Flow histograms show surface CLL1 and CD38 levels on AML blasts (CD33 + /CD34 +) from the PBMCs collected from 2 patients (Pt1 and Pt2). **E** The residual AML blasts were detected at 24 h or 72 h after co-culture with CLL1 CAR T cells at a 1:1 E:T ratio. Data represent 3 independent donors. *P* values were determined using one way ANOVA with Tukey's correction for multiple comparisons, or two-tailed, paired Student's *t* test for CAR vs CAR + SSR in residual AML blasts from Pt2 at 72 h. Bar graphs show mean + S.E.M. (*$P < 0.05$, **$P < 0.01$, ***$P < 0.001$. ns, non-significant).

anti-tumor control or animal survival in a MOLM13 xenograft model suggesting limited contribution of this mechanism in vivo. In contrast, incorporating a LAT endodomain dramatically potentiated the effect of SSR on cytotoxicity and T-cell expansion.

LAT plays a central role in TCR signal propagation. Phosphorylation of its four tyrosines by ZAP-70 creates docking sites for PLC-γ1 (pY^{132}) and adapter molecules GADS and Grb2 (pY^{171}, pY^{191} and pY^{226})[11,39,40]. PLC-γ1 cleaves PIP2 into IP3 and DAG which activate Ca^{2+} signaling and MAPK/NF-kB pathways, respectively. GADS binds to both pY^{171} and pY^{191} on LAT and facilitates recruitment of SLP-76, another scaffold molecule that activates Itk and HPK1 signaling. CAR tends to form an unstable and disorganized immune synapse with interspersed signal microclustering and poor actin-rich pseudoring[4]. Disrupting LAT expression did not abrogate CAR microcluster formation, suggesting an alternative activation complex bypassing LAT[41]. Our results, however, demonstrated ectopic expression of a LAT-based SSR can enhance CAR signaling suggesting a role of LAT in propagating CD3ζ signaling from a CAR.

A recent study demonstrated forced proximity of LAT and SLP-76 molecules ("Link CAR") was sufficient to activate T-cell effector function[13]. Further, full-length LAT endodomain attached to an extracellular targeting domain was sufficient to induce mild cytotoxicity due to spontaneous dimerization with SLP-76 via GADS; truncation of the LAT endodomain to remove both pY^{171} and pY^{191} required for GADS binding as well as pY^{226} that recruits Grb2 eliminated background cytotoxicity[13]. In our study, removing only pY^{191} and pY^{226} was sufficient to minimize SSR cytotoxicity against CD38+ target cells suggesting Y^{171} is insufficient for GADS-mediated recruitment of SLP-76. Therefore, truncation of the LAT endodomain was necessary to minimize CAR/TCR-independent cytotoxicity produced by the SSR thus ensuring a clean Boolean "AND" gate. However, if moderate cytotoxicity against the SSR target is tolerable (for example, if tumor cells express much higher levels of the SSR target compared to the normal tissue), a full-length LAT may be appropriate to provide an additional boost in cytotoxicity. Of note, replacing LAT in the SSR with a CD28 endodomain also produced non-specific cytotoxicity, possibly due to dimerization with a CAR-embedded CD28 domain. The exact mechanism of this activity remains to be elucidated. In contrast, utilizing TNFR superfamily endodomains 4-1BB and CD27 in the SSR impaired the expansion of T cells. This is likely a consequence of tonic TRAF2-mediated signaling that produces toxicity in T cells modified with gammaretroviral vectors and can be attenuated by using lentiviral or other self-inactivating/non-LTR vectors[18].

CD38 is a pan-hematopoietic antigens abundantly expressed in acute lymphoid and myeloid leukemia as well as in mature cell malignancies such as multiple myeloma and lymphoma[42]. Anti-CD38 monoclonal antibodies are an FDA-approved therapy for multiple myeloma with ongoing investigational clinical trials in other indications. CD38-directed antibody therapy can induce hematopoietic toxicity due to the expression of CD38 on normal blood cells and hematopoietic progenitors[43]. This also complicates the development of CD38-targeting CAR T-cell approaches and requires additional engineering to mitigate off-tumor toxicity[44]. Co-targeting CD38 with non-cytotoxic receptors helps avoid broadening the toxicity to normal tissues lacking CAR or TCR antigen while still leveraging high expression of CD38 on tumor cells. Further, efficient blocking of CD38 by the SSR on therapeutic T cells shields them from CD38 targeting thus enabling combinatorial therapy with CAR T cells and CD38-specific monoclonal antibodies.

More studies are needed to better understand factors regulating the activity and relative benefit of SSRs with other specificities and in other cancers. Our results indicate presence of the SSR target antigen on cancer cells is critical for the optimal activity suggesting co-localization of the antigen receptor and the LAT endodomain in the immune synapse is required to achieve highest signal amplification. Further, the level of the SSR target antigen expression can affect the degree of signal boost as we did not observe enhanced cytotoxicity against CLL1+ normal hematopoietic progenitors that express intermediate/dim levels of CD38 and saw no activity against a CD38dim KG1a line. Finally, the length of the extracellular spacer of the SSR and its target epitope may need to be matched with the antigen receptor to avoid exclusion from the synapse[45,46]. These and other factors may become important when developing SSRs for other targets and settings, such as solid tumors where high antigen heterogeneity is common. The lack of cytotoxicity elicited by the SSR allows targeting antigens highly expressed in solid cancers but also present in normal tissues, including EGFR, mesothelin, ephrins, and others.

Taken together, this study illustrates a strategy to enhance targeting tumor cells with suboptimal antigen expression using an additional synapse-stabilizing receptor. These results warrant additional investigation of the applicability of this approach beyond acute leukemias to improve outcomes in patients with antigenically heterogeneous cancers.

Methods

Cell lines

All leukemia cell lines are human-derived. THP1 (Male, TIB-202), HL60 (Female, CCL-240), KG1a (Male, CCL-246.1), and CCRF-CEM (Female, CCL-119) are from American Type Culture Collection (ATCC, Manassas, VA). Molm-13 (Male, ACC 554) and P12-ICHIKAWA (Male, ACC 34) are from Leibniz Institute DSMZ. Molm13, HL60 and KG1a were maintained in IMDM (Gibco™, Thermo Fisher Scientific) with 20% fetal bovine serum (FBS, Gibco™, Thermo Fisher Scientific). THP1, CCRF-CEM, P12-ICHIKAWA, T-ALL1 and BV173 were maintained in RPMI1640 (HyClone™, Cytovia) with 10-20% FBS. All media contained and 2mM L-GlutaMAX (Gibco™, Thermo Fisher Scientific). THP1-CLLlow was generated through sorting natural CLL1low cells from parental THP1 using SH800S Cell Sorter (Sony Biotechnology). Molm13-CD38KO was engineered by genetic knock-out of hCD38 using a CRISPR/cas9 system described below. All cell lines were subjected to Mycoplasma testing routinely, and have been authenticated with STR analysis in the Cytogenetics and Cell Authentication Core of MD Anderson.

Gene Knock-outs

sgRNA of *hCD38* (Target sequence: CGGTCTCGGGAAAGCGCT), *hCD3ε* (Target sequence: CACTCACTGGAGAGTTCT) and *hTRAC*

https://doi.org/10.1038/s41467-025-65897-4

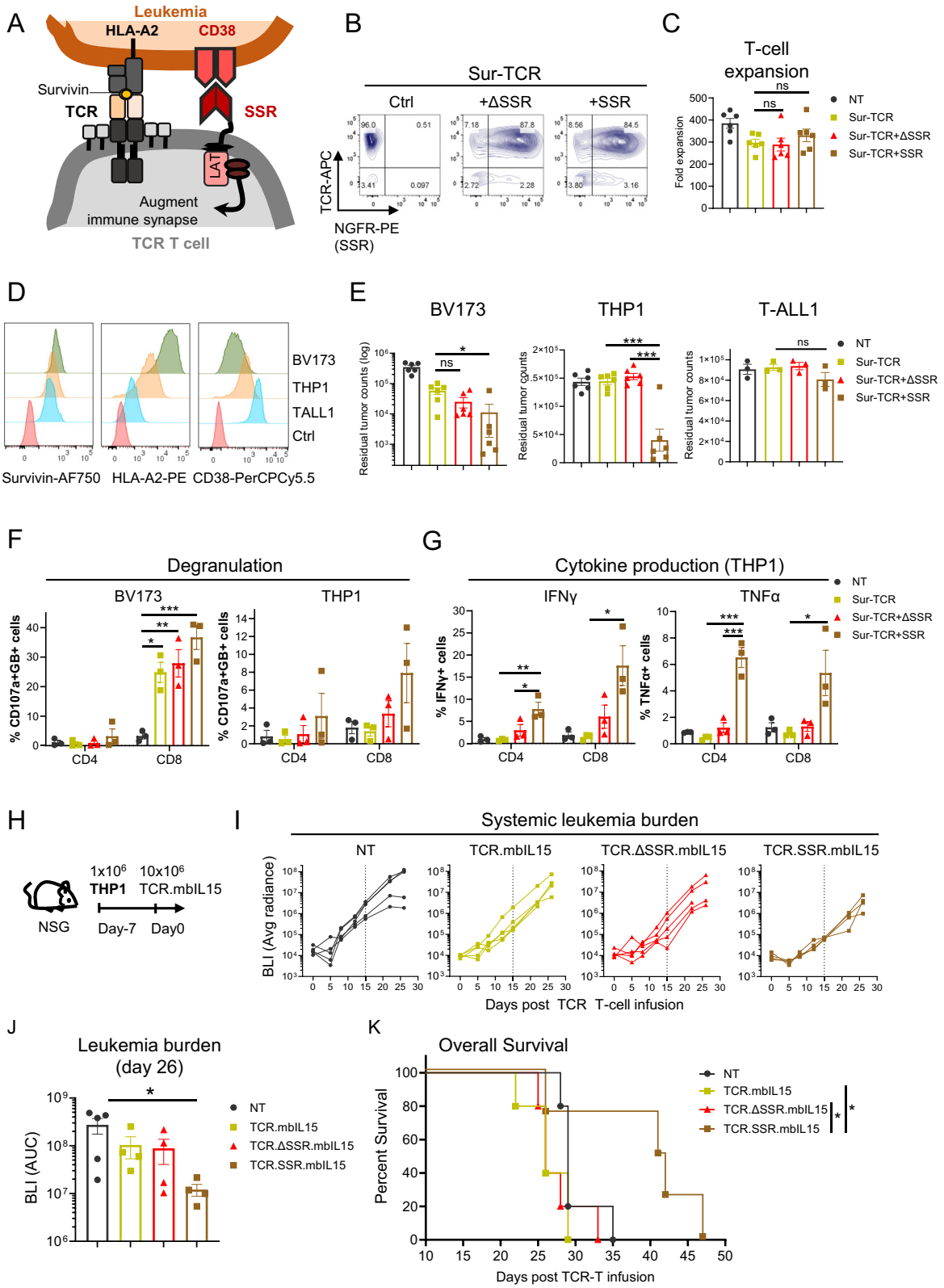

(AGTCTCTCAGCTGGTACA) were design using CRISPRscan and COSMID algorithms, and generated by an in vitro transcription system established previously[47,48]. For knock-out of *hCD38* in AML cell lines, briefly, 1 μg of CD38 sgRNA and 1 μg Cas9 protein (Integrated DNA Technologies) were electroporated into 0.25×10^6 Molm13 resuspended in 10 μl buffer R with one 1650-V, 20-ms pulse following the manufacturer's instruction of Neon Transfection System (Thermo Fisher Scientific). Residual CD38-positive Molm13 cells were further depleted using Magnetic MicroBeads (Miltenyi Biotech). For knock-out of *hCD3* and *hTRAC* in T cells, 1 μg of CD3ε sgRNA and 1 μg Cas9 protein were electroporated into 0.25×10^6 activated T cells at day 2 post-stimulation resuspended in 10 μl buffer T with three 1600-V, 10-ms pulses, and maintained in 2 ml CTL medium containing 20% FBS and 10 ng/ml IL7/IL15 overnight followed by retroviral transduction.

Fig. 6 | CD38.SSR potentiates leukemia targeting by Survivin-TCR T cells. A A schematic showing enhancement of cytotoxicity of survivin-specific TCR (Sur-TCR) by a CD38.SSR. **B** Representative flow plots showing co-expression of Sur-TCR and SSR on day 7 post-transduction (TD), and (**C**) expansion of TCR T cells derived from 3 HLA-A2- and 3 HLA-A2+ donors on day 10. Data represent 6 donors from two independent experiments. *P* values were determined using one way ANOVA with Tukey's correction for multiple comparisons. Bar graphs show mean + S.E.M. (ns, non-significant). **D** Histograms showing intracellular survivin, surface HLA-A2 and CD38 levels in leukemia cell lines BV173, THP1 and TALL1. **E** Residual tumor counts after a 3-day co-culture with Sur-TCR T cells at a 1:4 E:T ratio. Data represent 6 donors from two independent experiments in co-culture with BV173 and THP1, and 3 donors from one independent experiment in co-culture with TALL1. *P* values were determined using one way ANOVA with Tukey's correction for multiple comparisons. Bar graphs show mean + S.E.M. (*$P < 0.05$, **$P < 0.01$, ***$P < 0.001$. ns, non-significant). Percentages of (**F**) granzyme B/CD107a double positive T cells and (**G**) cytokine positive T cells after 4-h co-culture with indicated leukemia cells at 1:1 E:T ratio. Data represent 3 donors. *P* values were determined using one way ANOVA with Tukey's correction for multiple comparisons. Bar graphs show mean + S.E.M. (*$P < 0.05$, **$P < 0.01$, ***$P < 0.001$. ns, non-significant). **H** Schematic timeline of the mouse experiment. **I** Leukemia progression was monitored by bioluminescence. **J** Tumor burden AUC between day 0 and day 26. The data represent 5 mice in NT and 4 mice in for TCR, TCR.ΔSSR and TCR.SSR. *P* values were determined using one-way ANOVA with Dunnet's correction for multiple comparisons compared to NT. Bar graphs show mean + S.E.M. (*$P = 0.0394$). **K** Overall mouse survival in the THP1 model (NT, $n = 5$, TCR, $n = 5$, TCR.ΔSSR, $n = 5$, TCR.SSR, $n = 4$). Statistical significance was determined by a log rank test. (*$P = 0.0214$).

Constructs of SSRs and retrovirus production

CD38.SSRs were generated by Infusion Cloning (NEBuilder HiFi DNA Assembly, NEB) of synthesized dsDNA of CD38-specific single chain variable fragments (scFv) derived from anti-human CD38 mAb (Clone HB7, Patent No. 770718) with the PCR fragments of CD8α-hinge and transmembrane region including point mutation at C164S and the endo-domains of LAT (28–233a.a or 177a.a) amplified from a human complementary DNA library derived from T cells using CloneAmp HiFi PCR Premix (Takara Bio), followed by Sanger sequencing to confirm identity (Supplementary Fig. 16). CD38 CAR was generated by replacing the endodomain of SSRs with CD28 and CD3ζ domains from a cytotoxic CAR[49]. To clone GRP78.SSR, the extracellular domain of CD38. SSR was replaced with the PCR fragment of a GRP78-specific peptide CTVALPGGYVRVC fused with a mutant IgG4 hinge and a CD28 transmembrane domain amplified from GRP78.CAR[27]. Gammaretroviral vector (SFG) supernatant was made from 293 T cells as previously described[50]. Briefly, 0.6×10^6 293 T cells were seeded in a well of 6-well plates overnight, followed by transfection with 1.4 μg SFG vector, 1.4 μg Peg-Pam-e (MoMLV gag-pol proteins) and 1.1 μg RD114 (envelope protein) using a polyetherimide (PEI) transfection system under manufacturer's protocol (PEIpro®, Polyplus). The whole virus supernatant was collected at 48 h or 72 h post transfection and preserved at −80 °C for upcoming transduction.

T-cell activation and transduction

Activated T cells were generated by activating PBMC on 24-well plate pre-coated with 500 μl of 1 μg/ml OKT3 (Ortho Biotech, Bridgewater) and anti-CD28 antibodies (BD Biosciences) for 2 days in 2 ml CTL medium (45% Click's medium, 45% RPMI1640, 10% FBS and 2 mM L-GlutaMAX). Co-transduction was performed by pre-coating viral supernatant with the CLL1.CAR or Sur-TCR:CD38.SSR ratio 1:1 (1 ml) in RetroNectin (Takara Bio)-coated 24-well plate at 4122 g for 1 h at 32 °C, followed by removal of virus supernatant and spinoculation of 1×10^5 activated T cells in 1 ml CTL medium at 1000 g for 10 mins. The medium was replenished in the next day, and transduced T- cells were expanded and maintained in CTL medium containing 10 ng/ml recombinant human IL7 and IL15. T-cell growth and viability were assessed using Trypan Blue and a hemocytometer. T-cell phenotype was monitored by flow cytometry after T-cell transduction. CAR T cells were collected for functional analysis 7 days post transduction.

For generation of GRP78.SSR armed IL13Ra2.CAR T cells, sequential transduction was performed by transduction of 2.5×10^5 T cells with 500 μl IL13Ra2.CAR viral supernatant on day 2 and 500 μl GRP78.SSR viral supernatant on day 3 post T-cell activation, respectively. CAR expression and T cell phenotype were determined at 5 to 6 days post-transduction.

Co-culture and cytotoxicity assays

To examine the cytotoxicity of CAR and TCR T cells against leukemia cell lines, 20,000 target cells expressing green fluorescent protein and firefly luciferase (GFP.FFLuc) were co-cultured with 5,000 effector cells at a 1:4 E:T ratio without cytokines in each well of a flat-bottom 96-well plate. Residual tumor cells and effector cells were distinguished by GFP expression and quantified on day 0, day 1 and day 3 by flow cytometry using CountBright Counting Beads (Thermo Fisher Scientific), including 7-AAD (BD) to exclude dead cells. To measure cytotoxicity against CD38-postive primary cells, 0.2×10^6 autologous PBMCs isolated from health donors and labeled with 1 μM eFluor 670 (Invitrogen) were co-cultured with 50000 effector cells at 1:4 E:T ratio in 400 μl CTL medium (IL15/1L7 free) in each well of a flat-bottom 48-well plate. Purified NK cells were isolated using EasySep Human NK Cell Isolation Kit (STEMCELL). Residual efluor+ monocytes (CD14+), T cells (CD3+), NK cells (CD3-CD56+) and B-cells (CD19+) were quantified 24 h later by flow cytometry as described above.

To examine the cytotoxicity of IL13Ra2.CAR T cells against solid tumor cells in luciferase-based assays, 30,000 Firefly luciferase (ffLuc)-expressing tumor cells were seeded onto 96-well/white clear bottom plate (Thermo Fisher Scientific) and incubated with varying amounts of CAR T cells to assess cytotoxicity at a range of E:T ratios. Twenty-four hours later, the remaining tumor cells were quantified by luminescence when adding D-luciferin (Perkin Elmer) at 0.3 mg/mL in tumor media. Media only and tumor only served as controls to assess percent cytotoxicity. Luminescence was measured by using an Infinite200 Pro MPlex plate reader (Tecan, Männedorf, Switzerland).

Primary AML

For co-culture with primary AML blasts, 50,000 PBMCs isolated from patients with AML (recruited to the CARMEN study NCT04219163) were labeled with 1 μM eFluor 670 (Invitrogen), and co-cultured with 50,000 effector cells at 1:1 E:T ratio in 200 μl CTL medium (without cytokines) in each well of a flat-bottom 96-well plate. Residual efluor+ AML blasts (CD33 + CD34+) were quantified by flow cytometry. The study was conducted under an IND approved by the IRB and the FDA according to the principles of the Declaration of Helsinki. All participants gave informed consent prior to enrollment and any study procedures.

Colony formation assay

CD34+ cord blood (CB) cells sorted by Magnetic MicroBeads (Miltenyi Biotech) was a gift from the laboratory of Dr. Masataka Suzuki. Two thousand CD34 + CB cells were co-cultured with 20,000 effector cells in a flat-bottom 96 well plate for 5 h, followed by resuspended in 1 ml semi-solid methylcellulose gels containing recombinant cytokines required for colony formation of hematopoietic cells (H4434 Classic, MethoCult, STEMCELL) for 12 days. Colony formation of myeloid cells derived from CD34 + CB cells, including burst-forming units-erythroid (BFU-E) and colony-forming units-granulocyte, macrophage (CFU-GM), were identified and quantified under manufacturer's instruction.

Flow cytometry

In general, cells were stained with fluorochrome-conjugated antibodies in PBS (1% FBS) for 30 min at 4 °C, and after wash steps, all of samples were acquired by the Northern Lights™ flow cytometer (Cytek

Biosciences). Ultimately, the cell populations were gated and analyzed using FlowJo (BD Biosciences). Human BD Fc Block (BD Bioscience) was included for characterization of AML cell and PBMCs to reduce background of myeloid cells. The antibodies used in the studies are further categorized and listed below.

T-cell phenotyping: PE-NGFR (1:200) (clone C40-1457, BD, 557196), AF647-CLL1 CAR idiotype (1:200) (Clone MM162, Monoclonal Antibody Core, University of Texas M.D. Anderson Cancer Center), APC-mTCR beta (1:200) (clone H57-597, eBioscience, 17-5961-82), PerCPCy5.5-CD38 (1:100) (clone HIT2, BD, 551400), BV421-CD3 (1:200) (clone UCHT1, BioLegend, 300434), BV421-HLA-A2 (1:200) (clone BB7.2, BioLegend, 343326), PE-Cy7-CD4 (1:400) (clone L200, BD, 560644), FITC-CD8 (1:100) (Clone SK1, BD, 347313), V450-CCR7 (1:100) (clone 150503, BD, 560863), ECD-CD62L (1:200) (clone DREG56, IOTest, IM2713U), APC-AF750-CD45RA (1:200) (clone 2H4, IOTest, A86050), Alexa Fluor 647-AffiniPure Goat Anti-Mouse IgG, $F(ab')_2$ fragment specific (1:200) (Jackson ImmunoResearch, 115-606-006) and Alexa Fluor 647-G4S Linker (1:200) (clone E7O2V, Cell Signaling Technology, 69782).

Characterization of AML cell and PBMCs: BV421-CLL1 (1:200) (clone 50C1, BD, 74929), PerCP-Cy5.5-CD38 (1:100) (clone HIT2, BD, 551400), PE-HLA-A2 (1:100) (clone BB7.2, BioLegend, 343306), BV510-hCD45 (1:200) (clone HI30, BD, 563204), APC-CD3 (1:200) (Clone UCHT1, IOTest, IM2467U), PE-CD14 (1:100) (Clone MφP9, BD, 347497), FITC-CD56 (1:100) (Clone NCAM16.2, BD, 340723) and PE-Cy-CD19 (1:200) (clone SJ25C1, BD, 557835). The nuclear protein Survivin was stained with AF750-survivin (1:40) (clone 91630, R&D, IC886S) using True-Nuclear™ Transcription Factor Buffer set (BioLegend, 424401).

Intracellular staining: APC-IFNγ (1:100) (clone B27, BD, 554702), FITC-TNFα (1:100) (clone Mab11, BioLegend, 502906), BV-421-IL12 (1:100) (clone 5344.111, BD, 562914), APC-CD107a (1:100) (clone H4A3, BD, 641581) and V450-GzB (1:100) (clone GB11, BD, 561151).

Detection of cytokine production and degranulation of lytic granules

Molm13 target cells were co-cultured with 0.1×10^6 CAR T cells at 1:1 E:T ratio for 4 h at present of monensin (GolgiStop™ protein transport inhibitor BD Biosciences), followed by staining CD4 and CD8 surface markers for 30 min. Subsequently, the stained cells were fixed and permeabilized using BD Cytofix/Cytoperm (BD Biosciences) under manufacturer's instruction, and subjected to staining and analysis of IFNγ, TNFα, and IL2 and lytic granules (GranzymeB) by flow cytometry. For degranulation of lytic granules, the CD107a antibody was added into the T-cell medium during the 4-h co-culture for detection of the release of granules.

Confocal microscopy

The protocol for microscopic immune synapse characterization was established as previously described[51]. Poly-Lysine (PLL (Sigma-Aldrich, P4707))-coated coverslips were prepared using N1 coverslips (Thermo Fisher Scientific, 12-545-80 P) overnight at 4 °C. Then, they were washed with PBS and filled with media until Molm13 cells were seeded. Next, 100,000 Molm3 cells were plated onto the pre-coated coverslips and cultured for 30 mins at 37 °C/5% CO2. Then CAR T cells were added on top and co-cultured for 1 h at 37 °C/5% CO2. After co-culture, cells were washed with cold PBS and fixed with 4% paraformaldehyde (PFA, Electron Microscopy Sciences, 15710) for 10 min at room temperature. Fixed cells were washed twice with PBS, and the remaining PFA was inactivated with blocking buffer (PBS-2% BSA (Sigma-Aldrich, A9418) and 1.5 M glycine (Sigma-Aldrich, G8898)) for 10 min at room temperature. Cells were permeabilized by adding permeabilization buffer (PBS, 0.2% BSA and 0.05% saponin; Sigma-Aldrich, 47036) for 20 min at room temperature. Cells were washed twice with permeabilization buffer before primary antibody incubation and diluted in permeabilization buffer, following the manufacturer's instructions. All the primary antibodies were incubated at 4 °C overnight. Cells were washed with permeabilization buffer and incubated with secondary antibodies for 2 h at room temperature. Finally, cells were washed with permeabilization buffer and PBS before letting them dry for 1 h at room temperature. Then, coverslips were mounted onto slides using Fluoromount (Thermo Fisher Scientific, 00-4958-02).

Primary antibodies and probes with their dilutions are as follows: anti-human Lamp1 (1:50) (Abcam, ab25630); phalloidin-Alexa Fluor 647 (1:200) (Thermo Fisher Scientific, A22287); anti-pSLP76 (1:100) (Abcam, AB75829); anti-a-Tubulin (1:1000) (Abcam, ab6160); anti-GzB (1:100) (Cell signaling, 17215). Secondary antibodies with their dilutions are as follows: anti-rabbit Alexa Fluor 488 (1:200) (Thermo Fisher Scientific, A32731), anti-rat Alexa fluor plus 405 (Thermo Fisher Scientific, Cat#A48261), and anti-mouse Alexa Fluor 568 (1:200) (Thermo Fisher Scientific, A-11004).

Images were acquired in a Airyscan confocal microscope (Zeiss LSM 980), and the processing and analysis were performed with Fiji (ImageJ) software (Schindelin, J. et al. Fiji: an open-source platform for biological-image analysis. Nat. Methods 9, 676–682 (2012)). Single-cell images shown in the figures were cropped from a larger field. Image brightness and contrast were manually adjusted. To analyze lysosome and pSLP76 distribution in T cells, T cells were segmented by using celltrace violet signal, and the immune synapse was manually identified as the point of interaction between CAR T cells and tumor cells. To identify the polarization/recruitment of different labels, the center of mass of each fluorescence was identified and their relative distance from the IS was automatically calculated.

Live cell imaging of calcium influx

Tumor cells were labeled with CellTracker Red CMTPX (Invitrogen, Cat: C34552) or CellTrace Far Red (Invitrogen, Cat: C34564) (1:500) for 30 mins and then washed and maintained in culture media until image acquisition. 1×10^5 Molm13 cells were seeded onto PLL-coated μ-slide 8 well chambers (Ibidi, Cat: 80807) and 1×10^5 DIPG007 and DIPG7c cells were seeded onto the same chambers coated with GelTrex (Thermo Fisher Scientific, Cat: A1413302). Tumor cells were then incubated for 30 min at 37 °C and 5% CO2. 1×10^6 CAR T cells were resuspended in 1 mL of PBS and labeled with CellTrace Violet (1:1000) (Thermo Fisher Scientific, Cat: C34557) and CAL590 (ATTbioquest, Cat: 20510) or CAL520 (ATTbioquest, Cat: 21130) (1:500) for 1 h and then washed and maintained in T cell media until image acquisition. At a time of image acquisition, 1×10^5 CAR T cells were added to each well preloaded with tumor cells, and the image acquisition was initiated once T cells were detected in the visual field. Images were acquired in a spinning disc confocal microscope (Zeiss Axio Observer with CSU-X spinning disc), using a 63× objective. The acquisition parameters were a 4D image (60 min of acquisition with 1 min of frame, and 20 μm of height with a Z-step of 2 μm).

The processing and analysis were performed with FIJI (ImageJ) software48. Cell tracking49 and Ca2+ influx were performed using Trackmate plugin. All tumor and CAR T cell interactions were recorded over time, and Ca2+ influx was measured as the maximum fluorescence emitted by CAL520/590 signal which was normalized by its value before the first peak of calcium influx upon tumor interaction. Total Ca2+ influx was quantified as the area under curve. (AUC) of Ca2+ influx registry until 20 mins of interaction.

Western blotting

To investigate LAT downstream signaling, 1×10^6 CAR.SSR T cells were loaded into a well of a 24-well plate pre-coated with 0.3 μg anti-CLL1 CAR antibody and 1 μg recombinant human CD38 (Sino Biological, Cat: 10818) for 30 min on ice, followed by stimulation at 37 °C in a water bath for indicated time-points. Immediately, the stimulated T cells were harvested and lyzed with 100 μl RIPA buffer (Sigma-Aldrich, Cat:

R0278) containing the cocktail of proteinase/phosphatase inhibitors (Thermo Fisher Scientific, Cat:178440) for 30 min, and the protein lysates were collected after centrifugation at 8000 g for 10 mins. The protein samples were further prepared with 4x Laemelli buffer (Bio-Rad) with β-mercaptoethanol, and 20 µl of each sample was loaded into a well of 7.5 % or 10 % sodium dodecyl sulfate polyacrylamide gels for electrophoresis (SDS-PAGE, Bio-Rad) in parallel. Subsequently, the proteins were transferred into nitrocellulose (NC) membranes (Bio-Rad) and blocked in PBS with 0.2% Tween 20 and 5% skimmed milk for 1 h before antibody incubation. The NC membranes were incubated with primary antibodies at 4 °C overnight, followed by the incubation of secondary antibodies goat anti-mouse IRDye 680RD (1:5000) (LI-COR Biosciences, Cat: 925-68070) or goat anti-rabbit IRDye 800CW (1:10000) (LI-COR Biosciences, Cat: 925-32211) for 1 h at room temperature. Finally, the blots were developed using the LI-COR Odyssey CLx (LI-COR Biosciences) and quantified by ImageJ. The primary antibodies used are listed as follows: anti-phospho-LAT (Y132) (1:500) (Invitrogen, Cat: 44-224), anti-phospho-PLCγ1 (Y783) (1:500) (Cell Signaling Technology, Cat: 14008), anti-phospho-ERK1/2 (T202/Y204) (1:1000) (Cell Signaling Technology, Cat: 9101), anti-phospho-NFκB (S536) (1:500) (Cell Signaling Technology, Cat: 3033), and anti-GAPDH (1:3000) (Santa Cruz, Cat: sc-47724).

AML mouse xenograft models

Mouse work was performed using NSG-MHC class I/II DKO mice (NOD.Cg-Prkdc^{scid} H2-K1$^{b\text{-}tm1Bpe}$ H2-Ab1$^{g7\text{-}em1Mvw}$ H2-D1$^{b\text{-}tm1Bpe}$ Il2rg^{tm1Wjl}/SzJ, stock no. 025216) and NSG mice (NOD.Cg-Prkdc^{scid} Il2rg^{tm1Wjl}/SzJ, stock no. 005557), purchased from The Jackson Laboratory and bred separately in a pathogen free mouse room of Baylor College of Medicine animal facility. Mice were maintained under standard housing conditions.

To evaluate the efficacy of CAR.SSR T cells on antigen-low AML models, 0.5×10^6 Molm13-GFP/FFLuc cells or 1×10^6 THP1-CLL1^{low}-GFP/FFLuc cells were intravenously (i.v.) injected into each NSG-MHC class I/II DKO mouse aged 6-10 weeks (including both male and female), followed by infusion of CAR.SSR T cells expanded and collected at day7 post retroviral transduction 3 days after tumor engraftment. To evaluate the efficacy of Sur-TCR.SSR T cells on AML mice, 1×10^6, THP1-GFP/FFLuc cells were i.v. injected into each NSG-MHC class I/II DKO mouse, followed by infusion of 3 doses of 4×10^6 TCR.SSR T cells 7 days after tumor engraftment. 2000IU recombinant human IL2 (NIH) were intraperitoneally administered twice a week for the following three weeks after T-cell infusion. In experiments with Sur-TCR.SSR.mbIL15 T cells, 1×10^6 THP1-GFP/FFLuc cells were injected per mouse i.v., followed by a single dose of 10×10^6 TCR.SSR.mbIL5 T cells i.v. 7 days after tumor injection. The details of mouse age and sex in each experiment have been disclosed in the Source Data file.

Tracking total tumor burdens, each mouse was intraperitoneally administered with 100 µl D-luciferin (30 mg/mL; XenoLight, Revvity), and the bioluminescence imaging was detected after 10 mins using an IVIS Lumina II imaging system (Caliper Life Sciences), followed by quantification of radiance in Living Image software (Caliper Life Sciences). To track circulated tumor cells and T cells, 50 µl peripheral blood was obtained from the tail vein of mice, and red blood cells were removed by 1 ml RBC Lysis Buffer (BD Biosciences), followed by quantification of tumor counts (hCD45+GFP+) and CAR (hCD45+ CD3+ CAR+) or TCR (hCD45+ CD3+ TCR+) T-cell counts and phenotyping by flow cytometry using CountBright Absolute Counting Beads and 7-AAD. Mice showing signs of distress, immobility, disease progression, such as paralysis and distended abdomen, and/or weight loss exceeded 20% of baseline were euthanized in compliance with the Baylor College of Medicine IACUC (protocol AN-4758). CO2 euthanasia was conducted according to the IACUC-approved Euthanasia in Rodents Policy by use of automated CO2 euthanasia chambers with a SMARTBOX auto CO2 system (Euthanex, E-Z Systems).

Daratumumab-induced cytotoxicity

Twenty thousand CAR T cells were labeled by Cell Proliferation Dye eFluor 670 and co-culture with 60,000 NK cells purified by EasySep Human NK Cell Isolation Kit (STEMCELL) in presence of 10 µg/ml daratumumab (Selleckchem) or IgG1 isotype (BioXCell) control in 200 µl CTL medium for 4 h, followed by staining apoptotic cells with PB-annexinV (BioLegend) in Annexin V Binding Buffer (BioLegend), and analysis by flow cytometry.

Statistical analysis

Statistical analysis was performed and plotted using GraphPad Prism 10 software (GraphPad Software), and details are described in figure legends. In co-culture assays, data were pooled and analyzed with replica including T cells derived from different donors from independent experiments. The statistical significance between two groups was determined by two-tailed unpaired Student's *t test* in mouse experiments. The statistical analysis including multiple comparisons was performed using analysis of variance (ANOVA), and the *P* value was adjusted by Tukey's correction or Dunnett's correction. The difference between the two groups in a time course were calculated and compared by mean area under curve (AUC). The significance in Kaplan–Meier survival curves was determined by Mantel–Cox log-rank test.

Software

Data analysis was performed using indicated licensed software. Image in Fig. 2A was created in BioRender licensed under CC BY 4.0

Reporting summary

Further information on research design is available in the Nature Portfolio Reporting Summary linked to this article.

Data availability

The original data plotting the graphs and uncropped WB blots have been uploaded as a Source Data file, and supplementary data are provided in Supplementary information. Source data are provided with this paper.

References

1. Mardiana, S. & Gill, S. CAR T cells for acute myeloid leukemia: state of the art and future directions. *Front. Oncol.* **10**, 697 (2020).
2. Hou, A. J., Chen, L. C. & Chen, Y. Y. Navigating CAR-T cells through the solid-tumour microenvironment. *Nat. Rev. Drug Discov.* **20**, 531–550 (2021).
3. Wang, J. et al. CAR-T cells targeting CLL-1 as an approach to treat acute myeloid leukemia. *J. Hematol. Oncol.* **11**, 7 (2018).
4. Lindner, S. E., Johnson, S. M., Brown, C. E. & Wang, L. D. Chimeric antigen receptor signaling: functional consequences and design implications. *Sci. Adv.* **6**, eaaz3223 (2020).
5. Fry, T. J. et al. CD22-targeted CAR T cells induce remission in B-ALL that is naive or resistant to CD19-targeted CAR immunotherapy. *Nat. Med.* **24**, 20–28 (2018).
6. Majzner, R. G. et al. Tuning the antigen density requirement for CAR T-cell activity. *Cancer Discov.* **10**, 702–723 (2020).
7. Hazini, A., Fisher, K., Seymour, L. Deregulation of HLA-I in cancer and its central importance for immunotherapy. *J. Immunother. Cancer* **9**, e002899 (2021).
8. Majzner, R. G. & Mackall, C. L. Tumor antigen escape from CAR T-cell therapy. *Cancer Discov.* **8**, 1219–1226 (2018).
9. Zah, E., Lin, M. Y., Silva-Benedict, A., Jensen, M. C. & Chen, Y. Y. T cells expressing CD19/CD20 bispecific chimeric antigen receptors prevent antigen escape by malignant B cells. *Cancer Immunol. Res.* **4**, 498–508 (2016).
10. Rafiq, S., Hackett, C. S. & Brentjens, R. J. Engineering strategies to overcome the current roadblocks in CAR T cell therapy. *Nat. Rev. Clin. Oncol.* **17**, 147–167 (2020).

11. Gaud, G., Lesourne, R. & Love, P. E. Regulatory mechanisms in T cell receptor signalling. *Nat. Rev. Immunol.* **18**, 485–497 (2018).
12. Kabanova, A., Zurli, V. & Baldari, C. T. Signals controlling lytic granule polarization at the cytotoxic immune synapse. *Front. Immunol.* **9**, 307 (2018).
13. Tousley, A. M. et al. Co-opting signalling molecules enables logic-gated control of CAR T cells. *Nature* **615**, 507–516 (2023).
14. Hirabayashi, K. et al. Dual targeting CAR-T cells with optimal costimulation and metabolic fitness enhance antitumor activity and prevent escape in solid tumors. *Nat. cancer* **2**, 904–918 (2021).
15. Balagopalan, L., Coussens, N. P., Sherman, E., Samelson, L. E. & Sommers, C. L. The LAT story: a tale of cooperativity, coordination, and choreography. *Cold Spring Harb. Perspect. Biol.* **2**, a005512 (2010).
16. Zhang, W. et al. Association of Grb2, Gads, and phospholipase C-gamma 1 with phosphorylated LAT tyrosine residues. Effect of LAT tyrosine mutations on T cell angigen receptor-mediated signaling. *J. Biol. Chem.* **275**, 23355–23361 (2000).
17. Sandoval-Montes, C. & Santos-Argumedo, L. CD38 is expressed selectively during the activation of a subset of mature T cells with reduced proliferation but improved potential to produce cytokines. *J. Leukoc. Biol.* **77**, 513–521 (2005).
18. Gomes-Silva, D. et al. Tonic 4-1BB costimulation in chimeric antigen receptors impedes T cell survival and is vector-dependent. *Cell Rep.* **21**, 17–26 (2017).
19. Mamonkin, M. et al. Reversible transgene expression reduces fratricide and permits 4-1BB costimulation of CAR T cells directed to T-cell malignancies. *Cancer Immunol. Res.* **6**, 47–58 (2018).
20. Mihara, K. et al. Activated T-cell-mediated immunotherapy with a chimeric receptor against CD38 in B-cell non-Hodgkin lymphoma. *J. Immunother.* **32**, 737–743 (2009).
21. Han, X., Wang, Y., Wei, J. & Han, W. Multi-antigen-targeted chimeric antigen receptor T cells for cancer therapy. *J. Hematol. Oncol.* **12**, 128 (2019).
22. Tashiro, H. et al. Treatment of acute myeloid leukemia with t cells expressing chimeric antigen receptors directed to C-type lectin-like molecule 1. *Mol. Ther. J. Am. Soc. Gene Ther.* **25**, 2202–2213 (2017).
23. Ataca Atilla, P. et al. Modulating TNFalpha activity allows transgenic IL15-expressing CLL-1 CAR T cells to safely eliminate acute myeloid leukemia. *J. Immunother. Cancer* **8**, e001229 (2020).
24. Lee, H. C., Deng, Q. W. & Zhao, Y. J. The calcium signaling enzyme CD38 - a paradigm for membrane topology defining distinct protein functions. *Cell calcium* **101**, 102514 (2022).
25. Churchill, G. C. et al. NAADP mobilizes Ca(2+) from reserve granules, lysosome-related organelles, in sea urchin eggs. *Cell* **111**, 703–708 (2002).
26. Fang, C. et al. CD38 produces nicotinic acid adenosine dinucleotide phosphate in the lysosome. *J. Biol. Chem.* **293**, 8151–8160 (2018).
27. Ibanez, J. et al. GRP78-CAR T cell effector function against solid and brain tumors is controlled by GRP78 expression on T cells. *Cell Rep. Med.* **4**, 101297 (2023).
28. Krenciute, G. et al. Characterization and functional analysis of scfv-based chimeric antigen receptors to redirect T cells to IL13Ralpha2-positive glioma. *Mol. Ther. J. Am. Soc. Gene Ther.* **24**, 354–363 (2016).
29. Ostendorf, B. N., Flenner, E., Florcken, A. & Westermann, J. Phenotypic characterization of aberrant stem and progenitor cell populations in myelodysplastic syndromes. *PloS ONE* **13**, e0197823 (2018).
30. van Rhenen, A. et al. The novel AML stem cell associated antigen CLL-1 aids in discrimination between normal and leukemic stem cells. *Blood* **110**, 2659–2666 (2007).
31. Arber, C. et al. Survivin-specific T cell receptor targets tumor but not T cells. *J. Clin. Investig.* **125**, 157–168 (2015).
32. Hurton, L. V. et al. Tethered IL-15 augments antitumor activity and promotes a stem-cell memory subset in tumor-specific T cells. *Proc. Natl. Acad. Sci. USA* **113**, E7788–E7797 (2016).
33. Krenciute, G. et al. Transgenic expression of IL15 improves antiglioma activity of IL13Ralpha2-CAR T cells but results in antigen loss variants. *Cancer Immunol. Res.* **5**, 571–581 (2017).
34. Zhou, Y. et al. Interleukin 15 in cell-based cancer immunotherapy. *Int. J. Mol. Sci.* **23**, 7311 (2022).
35. Katsarou, A. et al. Combining a CAR and a chimeric costimulatory receptor enhances T cell sensitivity to low antigen density and promotes persistence. *Sci. Transl. Med.* **13**, eabh1962 (2021).
36. Haubner, S. et al. Cooperative CAR targeting to selectively eliminate AML and minimize escape. *Cancer cell* **41**, 1871–1891 e1876 (2023).
37. Kalaitsidou, M. et al. Signaling via a CD28/CD40 chimeric costimulatory antigen receptor (CoStAR), targeting folate receptor alpha, enhances T cell activity and augments tumor reactivity of tumor infiltrating lymphocytes. *Front. Immunol.* **14**, 1256491 (2023).
38. Omer, B. et al. A costimulatory CAR improves TCR-based cancer immunotherapy. *Cancer Immunol. Res.* **10**, 512–524 (2022).
39. Dinur-Schejter, Y., Zaidman, I., Mor-Shaked, H. & Stepensky, P. The clinical aspect of adaptor molecules in T cell signaling: lessons learnt from inborn errors of immunity. *Front. Immunol.* **12**, 701704 (2021).
40. Lin, J. & Weiss, A. Identification of the minimal tyrosine residues required for linker for activation of T cell function. *J. Biol. Chem.* **276**, 29588–29595 (2001).
41. Dong, R. et al. Rewired signaling network in T cells expressing the chimeric antigen receptor (CAR). *EMBO J.* **39**, e104730 (2020).
42. van de Donk, N. W. et al. Monoclonal antibodies targeting CD38 in hematological malignancies and beyond. *Immunol. Rev.* **270**, 95–112 (2016).
43. Casneuf, T. et al. Effects of daratumumab on natural killer cells and impact on clinical outcomes in relapsed or refractory multiple myeloma. *Blood Adv.* **1**, 2105–2114 (2017).
44. Glisovic-Aplenc, T. et al. CD38 as a pan-hematologic target for chimeric antigen receptor T cells. *Blood Adv.* **7**, 4418–4430 (2023).
45. Chang, V. T. et al. Initiation of T cell signaling by CD45 segregation at 'close contacts. *Nat. Immunol.* **17**, 574–582 (2016).
46. Davis, S. J. & van der Merwe, P. A. The kinetic-segregation model: TCR triggering and beyond. *Nat. Immunol.* **7**, 803–809 (2006).
47. Gomes-Silva, D. et al. CD7-edited T cells expressing a CD7-specific CAR for the therapy of T-cell malignancies. *Blood* **130**, 285–296 (2017).
48. Moreno-Mateos, M. A. et al. CRISPRscan: designing highly efficient sgRNAs for CRISPR-Cas9 targeting in vivo. *Nat. methods* **12**, 982–988 (2015).
49. Mamonkin, M., Rouce, R. H., Tashiro, H. & Brenner, M. K. A T-cell-directed chimeric antigen receptor for the selective treatment of T-cell malignancies. *Blood* **126**, 983–992 (2015).
50. Mo, F. & Mamonkin, M. Generation of chimeric antigen receptor T cells using gammaretroviral vectors. *Methods Mol. Biol.* **2086**, 119–130 (2020).
51. Ibanez, J. et al. Protocol for live-cell imaging of immune synapse formation and activation of CAR T cells against cancer cells. *STAR Protoc.* **5**, 103422 (2024).

Acknowledgements

The authors thank Caroline Porter and Dr. Masataka Suzuki for providing purified CD34+ cord blood cells; Dr. Lauren Scherer for providing the AML cell Molm13; Jack Tremblay for assistance with preparation of plasmids, and Daniil Shmidt for assistance with selection of primary AML samples. The study was funded by the CPRIT grant RP210158 and the SkyHigh Foundation to MM. PJC acknowledges the Young Investigator Award from Edward P Evans Foundation.

Author contributions

C.T.T. designed and executed experiments, analyzed and plotted data, and drafted the manuscript. J.I.V. characterized T-cell immune synapses and calcium influx of SSR T cells by performing confocal microscopic imaging and live imaging. PY assisted in setting up cytotoxicity assay and acquiring mouse samples and imaging for evaluation of CAR.SSR T-cell efficacy in vivo. R.T. developed GRP78 SSR and evaluated the in vitro activity of GRP78 SSR. NW cloned the constructs for initial selection of SSR binders and designed the construct of membrane bound IL15. T.H. and L.A.J.M. assisted in acquiring mouse samples and imaging for evaluation of TCR.SSR T-cell efficacy in vivo. M.V. cloned SSR with Y132F mutation and variant CLL1 CAR with different structures. PJC performed cell avidity measurement assays. G.K. facilitated microscopic characterization of immune synapses, designed GRP78 SSR, and analyzed data. M.M. conceptualized, funded, and directed the study, interpreted results, and drafted the manuscript.

Competing interests

M.M. is a co-founder with equity and an independent director at March Biosciences. M.M. receives fees from Allogene, Beam Therapeutics, Fate Therapeutics, March Biosciences, and Curie.bio. M.M. receives research support from Fate Therapeutics and March Biosciences and honoraria from Amgen and Galapagos NV and serves on the advisory board of NKILT Therapeutics and March Biosciences. M.M., N.W., G.K. and C.T.T. have patent applications in the field of engineered cell therapies. An up to date declaration of interests for the listed authors can be found at https://www.bcm.edu/academic-centers/cell-and-gene-therapy/research/disclosure-of-outside-interests. The remaining authors declare no competing interests.

Additional information

Supplementary information The online version contains supplementary material available at https://doi.org/10.1038/s41467-025-65897-4.

Correspondence and requests for materials should be addressed to Maksim Mamonkin.

Peer review information *Nature Communications* thanks Sebastian Kobold and the other, anonymous, reviewer(s) for their contribution to the peer review of this work. A peer review file is available.